

# New challenges for adaptive optics: extremely large telescopes

M. Le Louarn,<sup>1,2★</sup> N. Hubin,<sup>1★</sup> M. Sarazin<sup>1★</sup> and A. Tokovinin<sup>1★</sup>

<sup>1</sup>*European Southern Observatory, Karl Schwarzschild Str. 2, D-85748 Garching, Germany*

<sup>2</sup>*CRAL, Observatoire de Lyon, 9, Av. Charles André, F-69561 Saint Genis Laval, France*

Accepted 2000 March 30. Received 2000 March 27; in original form 1999 November 25

## ABSTRACT

The performance of an adaptive optics (AO) system on a 100-m diameter ground-based telescope working in the visible range of the spectrum is computed using an analytical approach. The target Strehl ratio of 60 per cent is achieved at 0.5  $\mu\text{m}$  with a limiting magnitude of the AO guide source near  $R$  magnitude  $\sim 10$ , at the cost of an extremely low sky coverage. To alleviate this problem, the concept of tomographic wavefront sensing in a wider field of view using either natural guide stars (NGS) or laser guide stars (LGS) is investigated. These methods use three or four reference sources and up to three deformable mirrors, which increase up to 8-fold the corrected field size (up to 60 arcsec at 0.5  $\mu\text{m}$ ). Operation with multiple NGS is limited to the infrared (in the  $J$  band this approach yields a sky coverage of 50 per cent with a Strehl ratio of 0.2). The option of open-loop wavefront correction in the visible using several bright NGS is discussed. The LGS approach involves the use of a faint ( $R \sim 22$ ) NGS for low-order correction, which results in a sky coverage of 40 per cent at the Galactic poles in the visible.

**Key words:** atmospheric effects – instrumentation: miscellaneous – telescopes.

## 1 INTRODUCTION

The current generation of large ground-based optical telescopes has primary mirrors with diameters in the 8- to 10-m range. Recently some thoughts have been given to the next generation optical telescopes on the ground. In these projects the diameter of the primary mirror lies in a range between 40 and 100 metres (see Mountain 1997; Gilmozzi et al. 1998; Andersen et al. 1999). The use of adaptive optics (AO, Roddier 1999) in the visible is crucial to obtain the full potential in angular resolution, to avoid source confusion for extragalactic studies at high redshifts, and to reduce the background contribution, dramatically increasing limiting magnitude (the signal-to-noise ratio is then proportional to the square of telescope diameter). Competition with space-based observatories, providing diffraction-limited imaging on an 8-m class telescope (see Stockman 1997) is also a driver for AO correction in the visible with larger apertures.

In this paper we address key issues for a visible light AO system on these extremely large telescopes (ELTs). We have chosen a telescope diameter of 100 m, since it represents the extreme case and we want to investigate the limiting factors of AO on such a large aperture. We shall not address here the astrophysical drivers for such an aperture size, which are presented elsewhere (Gilmozzi et al. 1998). We model the performance of an AO system working in the visible on a 100-m telescope, for an on-axis

natural guide star (NGS) (Section 2). The sky coverage with this approach is close to zero, because only bright objects ( $R \sim 10$ ) can be used as an AO reference. The use of a single artificial laser guide star (LGS) is ruled out by the huge error introduced by the cone effect or focus anisoplanatism (Foy & Labeyrie 1985). We propose to use turbulence tomography (i.e. 3D mapping of turbulence: Tallon & Foy 1990, hereafter TF90) combined with multi-conjugate adaptive optics (hereafter MCAO: see Foy & Labeyrie 1985; Beckers 1988) as a way to increase the fraction of the sky which can be observed. In Section 3 we present the main concepts involved in turbulence tomography. In Section 4 we describe a fundamental limitation of the corrected field-of-view size corrected by a small (1–3) number of deformable mirrors (DMs) and taking into account real turbulence profiles. A solution using three NGSS is presented, in which the correction is carried out in the visible (Section 5) and in the near-infrared (Section 6). In Section 7, another solution is presented, based on four LGSs for visible correction. In Section 8, we present and quantify some technical aspects of AO on ELTs. Finally, in Section 9, the conclusions are given.

## 2 AO PERFORMANCE WITH AN ON-AXIS NGS

There is a strong scientific interest in visible light studies with ELTs. Using the software described in Le Louarn et al. (1998) to perform analytical calculations of the AO system performance, we modelled a system with a Strehl ratio (ratio of the peak intensity of

★ E-mail: lelouam@eso.org (MLL); nhubin@eso.org (NH); msarazin@eso.org (MS); atokovinin@eso.org (AT)

the corrected image to the peak intensity of a diffraction limited image, hereafter SR) of 60 per cent at 0.5  $\mu\text{m}$ , based on a Shack–Hartmann wavefront sensor (e.g. Rousset 1994). The target SR is higher than required by the scientific goals,  $\sim 40$  per cent, to take into account potential error sources arising outside the AO system (e.g. aberration of the optics or co-phasing errors of the telescope primary mirror segments). Considering the current performance of AO systems, this is a challenging goal. However, the operation of ELTs is planned for some 10–20 years from now, and AO technology is bound to evolve considerably. The atmospheric model we used in these calculations corresponds to good observing conditions at the Very Large Telescope observatory of Cerro Paranal in Chile (Le Louarn et al. 1998). The main atmospheric parameters and the AO hardware characteristics are summarized in Table 1.

The effects of scintillation on the wavefront sensing were neglected. Preliminary studies (Rousset, private communication) have shown that the wavefront error contribution could be between 20 and 30 nm rms, reducing the SR by  $\sim 10$  per cent. The effects of the outer scale of turbulence were also neglected. Measurements (Martin et al. 1998) yield values usually between 20 to 30 m, significantly smaller than the diameter of the ELT. This is a new situation that cannot apply to current large telescopes. The effect of the outer scale is mainly to reduce the relative contribution of low-order modes of wavefront distortions (Sasiela 1994) and to decrease the stroke needed for the DM to several  $\mu\text{m}$ , independent of telescope diameter. This relaxes constraints on the design of DMs, but does not change the overall on-axis system performance.

The simulation results are presented in Fig. 1. The target SR of 60 per cent is obtained in the visible, providing a 1.03-mas diffraction limit at 0.5  $\mu\text{m}$ . The peak SR is over 95 per cent in the *K* band (2.2  $\mu\text{m}$ ), the diffraction limit being 4.5 mas. As a result of the fine wavefront sampling needed for correction in the visible, the limiting magnitude (at 0.5  $\mu\text{m}$ ) is  $R \sim 10$ , which is bright compared with current AO systems working in the near-infrared (around  $R \sim 16$ , e.g. Graves et al. 1998). This implies that with a single NGS the sky coverage is extremely small (see Rigaut & Gendron 1992 and Le Louarn et al. 1998 for a more extensive discussion on sky coverage with AO systems).

To overcome this limitation, we propose two different options, both involving multiple reference sources. NGS and LGS approaches are investigated in the following sections.

**Table 1.** AO simulation parameters. Atmospheric values are given at 0.5  $\mu\text{m}$ , WFS = wavefront sensor.

Telescope diameter	100 m
Number of actuators	$\sim 500\,000$
WFS readout noise	$1 e^-$
WFS quantum efficiency	90 per cent
WFS spectral bandwidth	500 nm
Transmission <sup>1</sup>	40 per cent
WFS subaperture size	16 cm
Max. WFS sampling rate	500 Hz
Seeing	0.5 arcsec
Coherence time	6 ms
Isoplanatic angle	3.5 arcsec

<sup>1</sup> Transmission of the atmosphere and telescope optics to the wavefront sensor. For visible light observations, light must be split between the wavefront sensor path and imaging path.

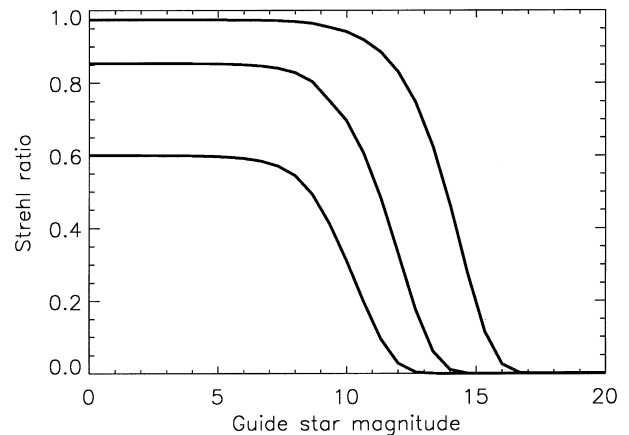


**Figure 1.** Strehl ratio versus magnitude at 0.5, 1.25 and 2.2  $\mu\text{m}$  (from bottom curve to top) for one on-axis NGS with the telescope pointing at zenith.

### 3 TURBULENCE TOMOGRAPHY

Turbulence tomography is a technique with which to measure the wavefront corrugations produced by discrete atmospheric turbulent layers with the help of several reference sources (TF90). Assuming weak turbulence, the phase corrugations produced by each layer add linearly (Roddier 1981). Knowing the configuration of the guide sources (position in the sky, height above ground in the case of an artificial star) and the altitudes of the layers to be measured, it is possible to reconstruct the phase at the selected turbulent layers. Foy & Labeyrie (1985) proposed using multiple DMs to correct them individually, a concept called multi-conjugate AO (MCAO). There must be at least as many measurements (number of guide stars times number of measurements points on the pupil) as there are unknowns (number of corrected layers times actuators on the correcting mirrors). Therefore, only a small number (2–4) of turbulent layers can be reconstructed, if a small number ( $\sim 4$ ) of reference sources are to be used. Recent papers have tackled the problems of turbulence tomography [TF90; Tallon, Foy & Vernin 1992; Ragazzoni, Marchetti & Rigaut 1999; Fusco et al. 1999; Le Louarn & Tallon (in preparation)], and reconstruction of turbulent wavefronts has been demonstrated in numerical simulations.

The maximum size  $\theta$  of the tomographic corrected field of view (FOV) is given by geometrical considerations,

$$\theta = \frac{D}{h_{\max}} \left( 1 - \frac{h_{\max}}{H} \right), \quad (1)$$

where  $D$  is the diameter of the telescope,  $h_{\max}$  is the height of the highest turbulent layer and  $H$  the height of the guide star (infinity for a NGS). As pointed out by TF90, in circular geometry, a small fraction of turbulence is not probed with this maximum FOV (pupil plane vignetting). This problem can be alleviated with a modal approach to turbulence tomography, which allows a slight interpolation of the wavefront within the corrected FOV (Fusco et al. 1999). With a 100-m telescope it may be possible to search reference stars in a much larger patch of the sky than with 8-m class telescopes. The probability of finding a reference source can be dramatically increased (Ragazzoni 1999). For a 100-m telescope, the maximum tomographic field is 17 arcmin in diameter with a NGS, or 13 arcmin for LGSs, if the highest turbulent layer is at 20 km above ground.

The image is corrected in the whole tomographic FOV only if the whole turbulence is concentrated in a few thin layers and if each layer is optically conjugated to its correcting mirror. Taking into account real turbulence profiles, we compute in the next section the FOV size which can be corrected with few DMs and we show that it is much less than the tomographic FOV.

## 4 LIMITATIONS OF MCAO

### 4.1 Turbulence vertical profile measurements

We have analysed the Paranal seeing campaign (PARSCA: Fuchs & Vernin 1993) balloon data on the vertical distribution of turbulence to test the assumption that all turbulence is concentrated within a few layers. During the site testing campaign, 12 balloons were launched at night to measure the profile of the refraction index constant,  $C_n^2(h)$ . Scintillation detection and ranging (SCIDAR: Azouit & Vernin 1980) measurements were also made simultaneously, confirming the balloon soundings (Sarazin 1996).

In Table 2 we summarize some parameters of the balloon flights. The average Fried parameter (Fried 1966),  $r_0$ , was 19 cm at 0.5  $\mu\text{m}$ , corresponding to a seeing of 0.55 arcsec – slightly better than the average seeing at Paranal, 0.65 arcsec. Considering the small time span during which the balloons were launched (19 d), these data are not fully representative of the site. The parameters have been corrected for the height difference between the observatory (2638 m), and the launching site (2500 m), which explains the slight difference with other publications (e.g. Sarazin 1996).

In Fig. 2 the  $C_n^2$  profiles obtained by the balloon flights are plotted. The height resolution of the balloons is  $\sim 5$  m. For clarity these measurements have been convolved with a Gaussian of standard deviation 500 m. The physics and formation of very thin turbulence laminae is described in Coulman, Vernin & Fuchs 1995. For most of the flights, the thin turbulent layers form larger structures which can be identified with the turbulent layers seen by SCIDAR (see for example the concentration of turbulence near 15 km on flight 45; altitudes are expressed in kilometres above sea level). The strongest of these layers is the boundary layer, in the first kilometres of the atmosphere, present on all plots. Another layer, present on most flights, is located near 10–12 km. These measurements confirm the existence of numerous layers. However, a continuous component of small but significant amplitude is also present on most of the soundings.

### 4.2 Anisoplanatism in MCAO

We used the high-resolution profiles (not convolved with a Gaussian) and applied the analytical formula derived by Tokovinin, Le Louarn & Sarazin (2000) to calculate the size of the FOV  $\theta_M$  which can be corrected with  $M$  deformable mirrors. This is a generalized isoplanatic angle in the sense of Fried (1982), expressed as

$$\theta_M = \left[ 2.905(2\pi/\lambda)^2 \int C_n^2(h) F_M(h, H_1, H_2, \dots, H_M) dh \right]^{-3/5}, \quad (2)$$

where  $F_M$  is a function depending on the conjugation heights of the DMs,  $H_i$  the height of conjugation above ground. This expression assumes that the correction signals applied to each DM are optimized. It assumes an infinite turbulence outer scale and an

**Table 2.** Balloon data for Cerro Paranal. The atmospheric coherence length,  $r_0$  and the isoplanatic angle  $\theta_0$ , are given at a wavelength of 0.5  $\mu\text{m}$ .

Flight	Date	Time	$r_0$ (m)	$\theta_0$ (")
38	10.03.92	3:30	0.32	3.80
39	11.03.92	4:45	0.15	4.09
40	12.03.92	1:30	0.21	3.58
43	14.03.92	2:45	0.07	0.42
45	15.03.92	1:00	0.19	2.05
46	15.03.92	5:00	0.22	1.74
48	16.03.92	4:10	0.17	2.48
50	24.03.92	8:12	0.13	1.66
51	25.03.92	2:43	0.23	2.03
52	25.03.92	7:11	0.21	2.22
54	23.03.92	4:10	0.22	2.81
55	29.03.92	9:15	0.14	1.65

infinite  $D/r_0$  ratio. For 1 DM conjugated to altitude  $H_1$ , equation (2) contains

$$F_1(h) = |h - H_1|^{5/3}, \quad (3)$$

which reduces to  $F_1(h) = h^{5/3}$  if  $H_1 = 0$  as in conventional AO and yields the classical  $\theta_0$ . For a two-mirror configuration the function has the form

$$F_2(h, H_1, H_2) = 0.5[|h - H_1|^{5/3} + |h - H_2|^{5/3} - 0.5|H_2 - H_1|^{5/3} - 0.5|H_2 - H_1|^{-5/3}(|h - H_1|^{5/3} - |h - H_2|^{5/3})^2]. \quad (4)$$

For three or more DMs the expression for  $F_M$  is much more complex. The heights  $H_i$  were computed with a multiparameter optimization algorithm to maximize  $\theta_M$ . We explored the possibilities with one, two and three DMs in different altitude combinations, from all  $H_i$  fixed to all  $H_i$  optimized. In the optimized setups, the heights of the mirrors were adapted for each flight to maximize the isoplanatic angle. For fixed DMs, we chose the conjugation height as the median of the heights found by optimization. The DM configurations are summarized in Table 3, and our results are shown in Fig. 3.

With three DMs, the increase in  $\theta_3$  (compared to  $\theta_0$ ) ranges from a factor of 2.6 to a factor of 13, depending on the profile. The median increase of  $\theta_3$  is a factor of 7.7, which means that the isoplanatic angle in the visible increases from 2.2 to 17 arcsec. On particular nights (Flight 43 for example, which has a lot of extended high-altitude turbulence)  $\theta_3$  stays small,  $\sim 6$  arcsec. The largest  $\theta_3$  found was 28.9 arcsec (Flight 38). A wavelength of 2.2  $\mu\text{m}$  yields a median  $\theta_3$  of 102 arcsec (for comparison,  $\theta_0 = 13$  arcsec). A two-mirror configuration brings improvement factors between 1.6 and 8.7, with a median of 4.6. Therefore, with two DMs, one can expect to increase the isoplanatic angle to  $\sim 10$  arcsec in the visible. Adapting the conjugate height of the DMs to profile variations is not crucial ( $\theta_3$  increases only by  $\sim 7$  per cent when using three optimized heights instead of fixed ones). Fig. 4 shows the optimal conjugate heights for the DMs as a function of flight number. Three main heights are identified: ground,  $\sim 10$ –12 km and 15–20 km. Considering the observed stability of the optimum heights (as a result of the stability of the main turbulent layers), it is not surprising that optimizing the heights does not significantly improve the FOV. Notice the large

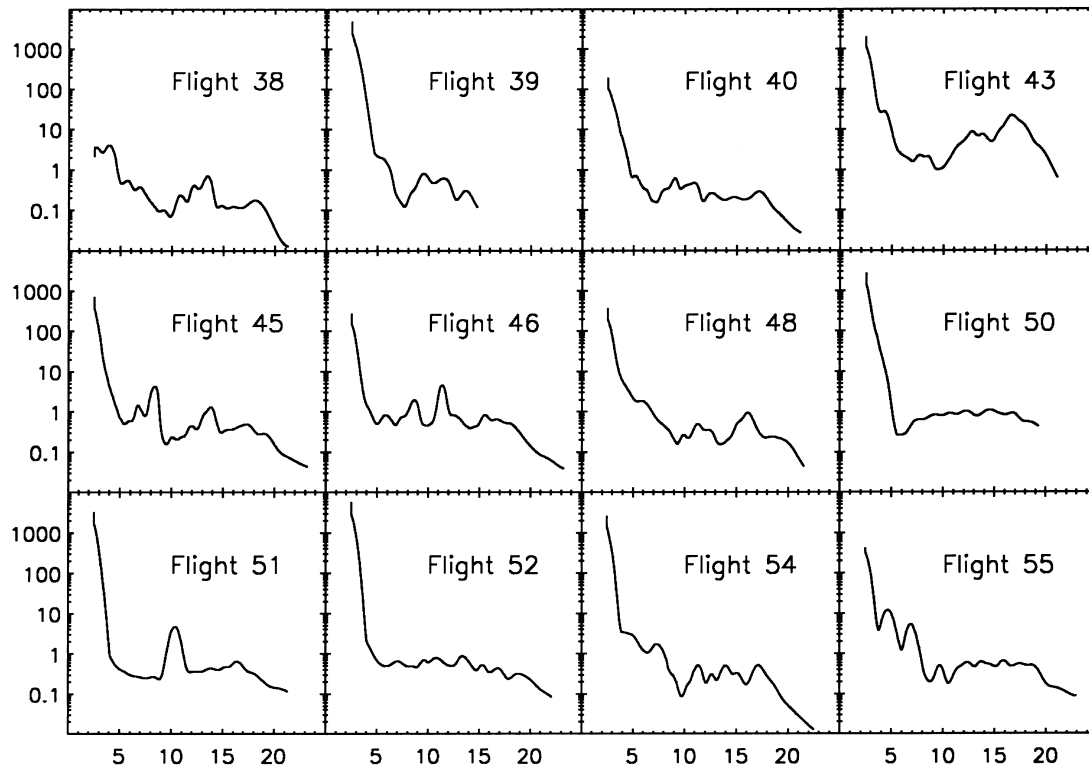


**Figure 2.** Profiles obtained by balloon soundings above Cerro Paranal, smoothed with a Gaussian of standard deviation 500 m. The abscissae are altitudes in kilometres above sea level. Ordinates are the refractive index structure constant ( $C_n^2$ ) in units of  $10^{-17} \text{ m}^{-2/3}$ .

**Table 3.** MCAO configurations and optimization results for Cerro Paranal. The columns contain:  $N$  – configuration number (same as in Fig. 3),  $M$  – number of DMs,  $H_1, H_2, H_3$  – median conjugate heights of the DMs above sea level,  $\theta_M$  – median isoplanatic angle in arcsec at  $0.5 \mu\text{m}$ ,  $G$  – gain in  $\theta_M$  compared to the median  $\theta_0$ ,  $G_{\min}$  – minimum gain in  $\theta_M$ ,  $G_{\max}$  – maximum gain in  $\theta_M$ .

$N$	$M$	$H_1, \text{m}$	$H_2, \text{m}$	$H_3, \text{m}$	$\theta_M, ''$	$G$	$G_{\min}$	$G_{\max}$
1	1	F: 2638	–	–	2.20	1		
2	1	O: 5722	–	–	3.04	1.27	1.14	1.98
3	2	F: 3705	F: 15337	–	10.00	4.50	1.39	8.55
4	2	F: 3381	O: 15337	–	10.30	4.63	1.55	8.29
5	2	O: 3705	O: 15337	–	10.38	4.66	1.66	8.68
6	3	F: 3381	F: 10875	F: 17922	15.96	7.17	2.17	11.80
7	3	F: 3381	F: 10875	O: 18030	16.04	7.20	2.25	11.80
8	3	F: 3381	O: 11041	O: 17842	16.61	7.46	2.38	12.18
9	3	O: 3381	O: 10875	O: 17922	17.23	7.74	2.56	12.97

O – optimized altitude, maximizing the isoplanatic angle.

F – fixed altitude, taken to be the median of the optimized heights.

deviation for point 2 (Flight 39). As shown in Fig. 2, the turbulence was located very low, and the balloon reached only a maximum altitude of  $\sim 15$  km, leaving part of the turbulence unmeasured.

These results show that anisoplanatic effects occur in the visible even with three DMs used in an MCAO approach. They represent only one site, on a relatively short time-scale. Other sites with similar isoplanatic angles exist (e.g. the measurements at Maidanak, Uzbekistan, provide a median  $\theta_0$  of 2.48 arcsec: Ziad et al, in preparation). Moreover, the  $\theta_M$  computed here is somewhat pessimistic, since it contains a piston term (which reduces the isoplanatic angle but does not affect image quality) and does not take into account the finite number of corrected

turbulent modes. This is similar to the effect seen with  $\theta_0$ , which overestimates isoplanatic effects (Chun 1998). Therefore, it is reasonable to expect a corrected FOV between 30 and 60 arcsec in diameter, in the visible. This is a considerable improvement over the few arcsec isoplanatic field in the visible (roughly equal to  $\theta_0$ ), but much less than the tomographic FOV given by equation (1).

We suggest that the site where an ELT is built be optimized in terms of turbulence profiles, and not only in terms of total turbulence, as used to be the case in previous surveys.

It is more effective to correct a few strong layers (even if the total turbulence is higher) than to have to correct for a continuous repartition of lower amplitude turbulence. Indeed, comparing (for example) Flights 46 and 55 shows that a similar  $\theta_0 \sim 1.7$  arcsec

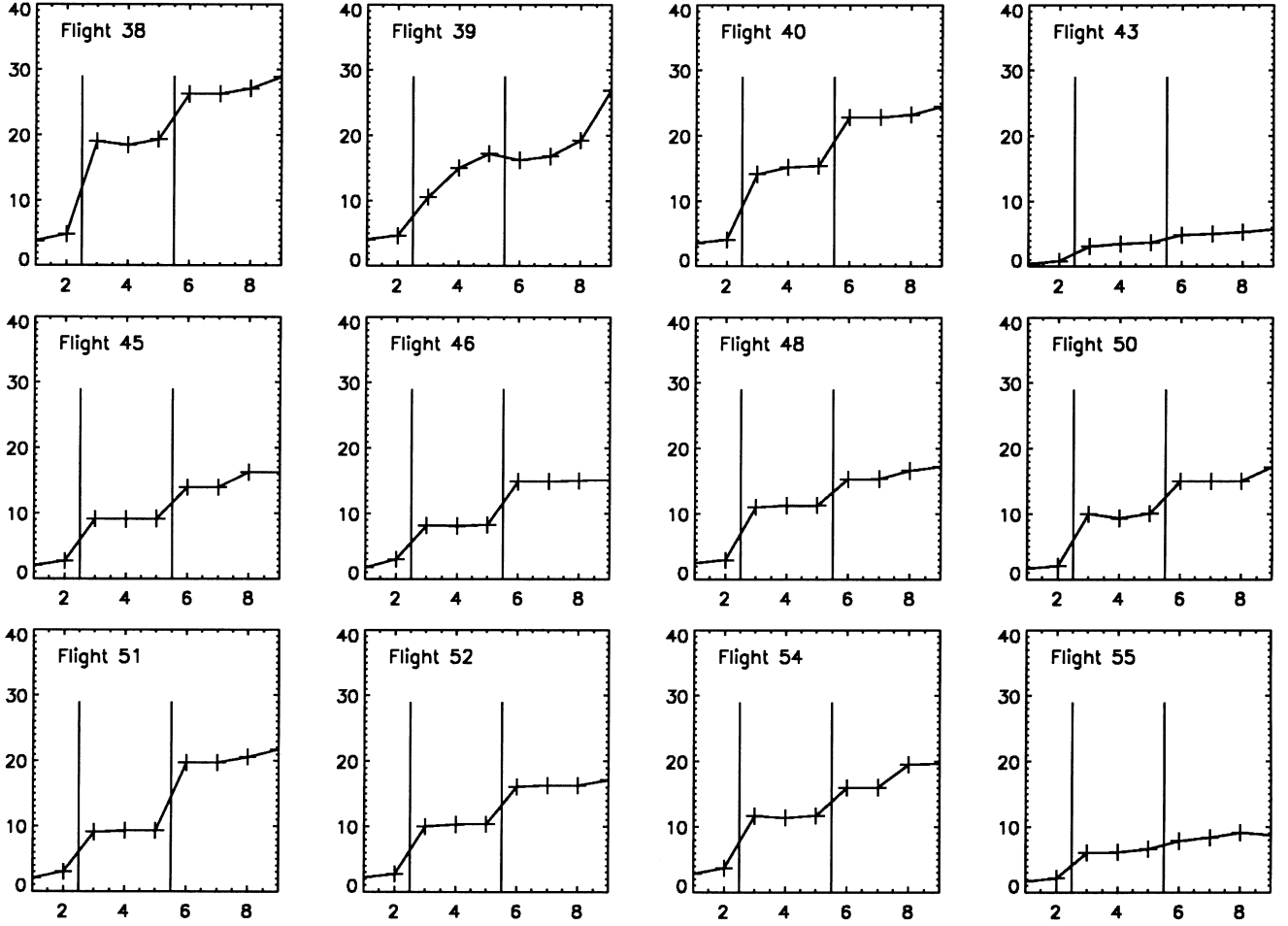


**Figure 3.** Isoplanatic angles ( $\theta_M$ , ordinate axis, in arcsec at  $0.5 \mu\text{m}$ ) for different DM configurations (in abscissa, corresponding to  $N$  in Table 3). Configurations 1, 2 are for a single DM, 3–5 for two DMs and 6–9 for three DMs.

can be well corrected with three DMs (Flight 46,  $\theta_3 \sim 14$  arcsec) if turbulence is concentrated in a few peaks (see Fig. 2), whereas a quasi-continuous turbulence benefits much less from MCAO correction (Flight 55,  $\theta_3 \sim 9$  arcsec). The location of the turbulent layers should also be as stable as possible, to minimize the changes in DM conjugate height. Of course, some other parameters of the site will have impact on the telescope performance, e.g. the wind (which is likely to be an important factor on such a large structure).

### 4.3 Required field of view

In tomographic wavefront sensing using LGSs, the reference sources are placed at the edges of the corrected field (TF90). Therefore with three DMs the LGSs are positioned  $\theta_{\text{LGS}} = \theta_3$  apart. The telescope FOV,  $\theta_{\text{tel}}$ , must, however, be larger (see Fig. 5) for the laser spots to be imaged by the telescope:

$$\theta_{\text{tel}} = \theta_{\text{LGS}} + \frac{D}{H}. \quad (5)$$

For a 100-m telescope and a sodium LGS placed at a 90 km height, and for  $\theta_{\text{LGS}} = 60$  arcsec, we get  $\theta_{\text{tel}} = 290$  arcsec, or almost 5 arcmin in diameter. This can be a severe requirement for the telescope optical design.

## 5 NATURAL GUIDE STARS FOR VISIBLE CORRECTION

The use of several NGSs on an ELT to increase the corrected FOV and to find reference stars outside the isoplanatic patch was proposed by Ragazzoni (1999). He pointed out that, with

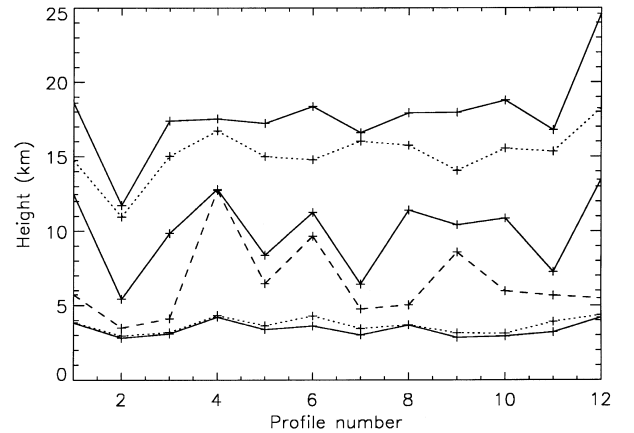


**Figure 4.** Optimized conjugate heights of the DMs (in kilometres) as a function of profile number. Solid line is for the 3 DM configuration, dots for the 2 DM configuration and dash is for a single DM.

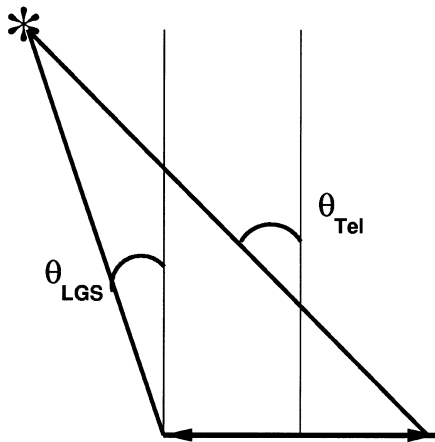


**Figure 5.** Required telescope field of view  $\theta_{\text{Tel}}$  compared to the corrected field  $\theta_{\text{LGS}}$  which corresponds to the positions of the LGS. The need for a FOV much larger than  $\theta_{\text{LGS}}$  is evident.

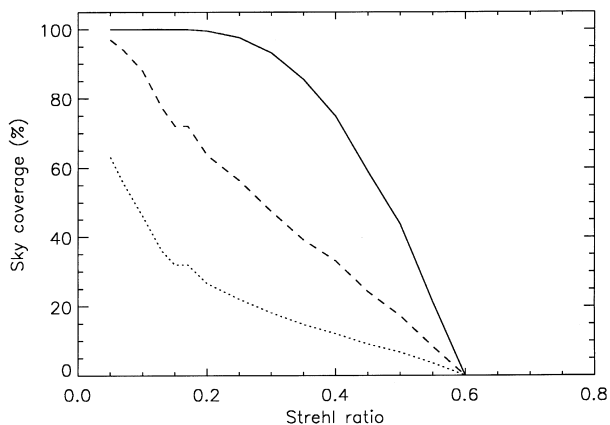


**Figure 6.** Sky coverage at  $0.5 \mu\text{m}$  using three NGSs in a corrected FOV of 12 arcmin in diameter if wavefront sensing can be done in open loop. From top to bottom curve: (solid) near Galactic plane, (dash) average latitude, (dot) near Galactic pole.

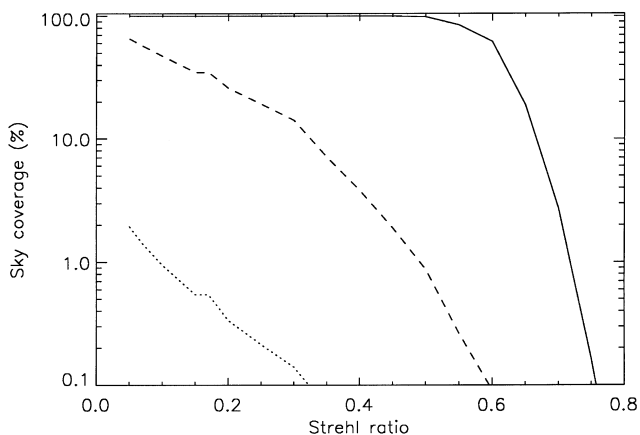


**Figure 7.** Sky coverage in the J band using three NGSs with a corrected FOV of 3 arcmin in diameter. From top to bottom curves: (solid) near Galactic plane, (dash) average latitude, (dot) near Galactic pole. Notice the logarithmic scale of the ordinate axis.

turbulence tomography, the maximum FOV which can be corrected increases linearly with telescope diameter, as shown by equation (1). Therefore, it would be possible to use the huge tomographic FOV to search for natural references. This work assumed that anisoplanatism was not present in turbulence tomography (turbulence concentrated in a few thin layers). In the previous paragraph we have shown that this is unfortunately not the case with real turbulence profiles. As a consequence, if the reference stars are much further away than  $\theta_M$  they will not benefit from AO correction. The wavefront measurement would therefore be done in open loop. This is a very unusual situation in AO (Roddier 1999), and experiments must be carried out to verify the feasibility of that approach.

Moreover, our further studies show that for widely separated NGSs, the errors of tomographic wavefront reconstruction with real turbulence profiles can be very high. So the use of three NGSs in a wide tomographic field seems problematic. Still, we estimate the sky coverage for this option.

Another constraint comes from the telescope design. The telescope FOV of an ELT is a strong cost driver and, at the moment, a full tomographic FOV (17 arcmin) does not seem to be feasible. Current optical designs for a 100-m telescope (Dierickx et al. 1999) provide a maximum FOV of 12 arcmin.

We have computed the sky coverage (SC) for the case when reference stars are sought within a 12 arcmin FOV (Fig. 6). Full SC is obtained only near the Galactic plane. A 60 per cent SC can be achieved with a SR of 0.2 at average Galactic coordinates ( $l = 180^\circ$ ,  $b = 20^\circ$ ), or 30 per cent near the pole.

If a telescope design can be improved to have the maximum FOV allowed by tomography (equation 1), the SC will be significantly increased. A full SC can be achieved with a SR of 0.1 everywhere. SC of 50 per cent is achieved on the whole sky with a SR of at least 0.4. Given the performance of the AO system shown in Fig. 1, the telescope FOV size is identified here as a limiting factor for the sky coverage.

Initially we presumed in these simulations that the limiting magnitude for three NGSs is the same as for one NGS, e.g.  $R \sim 10$  (Fig. 1). This is conservative with regards to the results obtained by Johnston & Welsh (1994): when using four reference stars, the flux from the individual reference sources could be divided by four, i.e. a gain of 1.5 mag. We have therefore also studied the cases in which the limiting NGS magnitudes were one and two magnitudes fainter. Such gains could be achieved by efficient tomographic reconstruction algorithms. If the limiting magnitude can be increased by 1 mag, a SC of 40 per cent at the Galactic pole and 90 per cent at average Galactic latitudes can be obtained with a SR of 0.2. With the maximum tomographic FOV, a SC of 50 per cent is obtained with a SR 0.5 at the Galactic pole.

## 6 NATURAL GUIDE STARS AND CORRECTION IN THE INFRARED

The main problem of the NGS approach in the visible is caused by residual anisoplanatism. This problem is alleviated when only correction in the infrared is needed. At  $1.25 \mu\text{m}$ ,  $\theta_M$  is increased by a factor of 3 compared to the visible (see equation 2). For  $\sim 60$  arcsec FOV in the visible (diameter), a 3-arcmin corrected FOV is obtained. The limiting magnitude, as shown by Fig. 1, increases from  $R \sim 10$  to  $R \sim 13$ . The sky coverage is plotted in Fig. 7. It shows that with a Strehl ratio of 0.2, SCs of 0.4, 30 and 100 per cent are obtained respectively at Galactic poles, at average

latitudes and in the Galactic disc. If a 1-mag gain in limiting magnitude is obtained compared to a single NGS, the coverages increase only slightly.

At  $2.2\ \mu\text{m}$ , the FOV is  $\sim 6$  arcmin (diameter) and the limiting magnitude is about  $R \sim 15$ . The sky coverage is 10 per cent at the Galactic pole and complete elsewhere.

## 7 LASER GUIDE STARS

For astronomical AO systems, LGSs based on resonant scattering in the sodium layer (Foy & Labeyrie 1985) are usually considered because they provide the highest reference source available, reducing the cone effect (also called focus isoplanatism: Foy & Labeyrie 1985; Fried & Belsher 1994; Tyler 1994). This effect is as a result of the finite altitude of the laser guide star. It currently prevents the use of high AO correction in the visible with 8-m telescopes.

### 7.1 Power requirements

The laser power requirements for current AO systems working in the near-IR is of about 5 W (continuous wave, CW), providing LGS brightness equivalent to a  $\sim 9$ -mag guide star (Jacobsen et al. 1994; Max et al. 1997; Davies et al. 1998). The typical subaperture size for those systems is 60 cm. Scaling to the subaperture size in the visible (16 cm) to obtain similar performance, the power of the laser should be 14 times higher (assuming a linear scaling of the guide star brightness with laser power), or about 70 W (CW). This scaling does not take saturation of the sodium layer into account. Milonni, Fugate & Telle 1998 provide an analytical tool with which to compute the power requirement in the case of a pulsed laser for a given guide star brightness with saturation. Using pulsed laser characteristics of the Keck LGS implementation (Sandler 1999) – 11-kHz repetition rate, 100-ns pulse duration, – we infer that to receive the same number of photons as for a 70 W CW laser, a  $\sim 175$  W pulsed laser is needed. However, considering Fig. 1, we can see that a 9-mag guide star would provide a Strehl ratio of 40 per cent. Therefore, if a slight loss of the AO system performance is acceptable, a significantly smaller amount of laser power would be sufficient.

One could instead use a Rayleigh-scattering based LGS system (Fugate et al. 1994). This has the advantage of being able to use any laser (producing a bright LGS at an arbitrary wavelength is currently not a problem, see Fugate et al. 1994). However, the low altitude of Rayleigh LGSs ( $\sim 15$  km) reduces its suitability for tomography. The position of the LGSs to obtain a zero-corrected FOV (only the cone effect is removed) is

$$\theta_{\text{null}} = \frac{D}{H}. \quad (6)$$

$\theta_{\text{null}} \sim 23$  arcmin ( $D = 100$  m,  $H = 15$  km), whereas the maximum tomographic FOV (equation 1) allowed by the highest turbulent layer (10 km, optimistic considering Fig. 2) is  $\sim 11$  arcmin (for a guide star placed at 15 km). Therefore, the cone effect cannot be fully corrected with only four Rayleigh LGSs on ELTs and we will not consider this option in the remainder of this paper.

### 7.2 Multiple sodium laser guide stars

On a 100-m telescope, the use of a single LGS is totally impossible because of the huge cone effect involved. The option

of using multiple (4) sodium laser guide stars in a tomographic fashion has therefore been investigated. We should stress that LGSs are placed on the edges of the corrected FOV (TF90), and therefore the problem of open-loop wavefront measurements does not affect this approach (the required FOV is given by  $\theta_M$ ). The problem with LGSs in turbulence tomography is that the wavefront tilt cannot be obtained from the LGS (Pilkington 1987) and propagates into the global reconstructed wavefront. In addition to global tilt, other low-order modes (like forms of defocus and astigmatism) have to be measured from an NGS located in the reconstructed FOV (Le Louarn & Tallon, in preparation). Elaborate techniques have been proposed to measure the tilt from the LGS (see e.g. Foy et al. 1995; Ragazzoni 1996). Unfortunately, real-time correction has not been demonstrated. If tilt can be retrieved, this problem disappears and full SC is achieved.

To solve the problem of LGS tilt indetermination, we propose to use in conjunction with LGS a very low-order wavefront sensor (for example a curvature sensor, Roddier, Roddier & Roddier 1988) working on a faint NGS. The limiting magnitude with 19 subapertures (4 subapertures across the pupil) is currently of  $R \sim 17$  (Rigaut et al. 1998) on a 3.6-m telescope, with correction at  $2.2\ \mu\text{m}$ . In Table 4, we summarize the scaling factors to be taken into account to convert this limiting magnitude to that of a 100-m telescope with a correction in the visible. The limiting magnitude is  $R \sim 22$ . This scaling is only valid if compensation is done in the visible, so that wavefront sensing benefits from the AO correction (Rousset 1994). Otherwise, as shown by Rigaut & Gendron (1992), there is no gain in limiting magnitude for low-order wavefront sensing on a large aperture compared to 4-m class telescopes.

We used a model of the Galaxy developed by Robin & Cr ez e (1986) to get the probability to find a star of a given magnitude within a given FOV. Considering the faint magnitudes this system will be able to use, we also took into account the density of galaxies in the sky. We used galaxy counts given by Fynbo, Freudling & Moller (1999), based on a combination of measurements from the *Hubble Deep Fields* (north and south: Williams et al. 1996) and the ESO New Technology Telescope deep field, Arnouts et al. 1999). Near the Galactic pole, galaxies become more numerous than stars for magnitudes fainter than  $R \sim 22$ . A

**Table 4.** Scaling of curvature sensor limiting magnitude from a 3.6-m telescope with a correction at  $2.2\ \mu\text{m}$  to a 100-m at  $0.5\ \mu\text{m}$ .  $D_{100}$  is the 100-m telescope diameter,  $D_{3.6}$  the 3.6-m diameter.  $r_0$  is given in the visible ( $\sim 0.2$  m).  $\lambda_{0.5}$  is the correction wavelength of the ELT,  $\lambda_{2.2}$  the correction wavelength of the 3.6-m telescope. The factor 19 is the number of subapertures on both pupils.

Factor	Flux gain (mag)
Diameter $\propto \left(\frac{D_{100}}{D_{3.6}}\right)^2$	+7
Coherence time $\propto \left(\frac{\lambda_{2.2}}{\lambda_{0.5}}\right)^{6/5}$	-2
Measurement precision $\propto \frac{1}{19} \left(\frac{D_{100}}{r_0}\right)^2$	+10
Required precision $\propto \left(\frac{D_{3.6} \lambda_{0.5}}{D_{100} \lambda_{2.2}}\right)^2$	-10
Total	5

bias may exist since not all of these galaxies can be used as a reference because of their size (a source size smaller than 4 mas was assumed in Table 4). However, usually, the fainter the galaxies the smaller they are. We have assumed that galaxies are distributed evenly in the sky. Poisson statistics give the probability of finding a reference object for a given AO limiting magnitude.

In Fig. 8 the probability of finding an NGS within a field of 30 arcsec in diameter is shown. The SC is  $\sim 13$  per cent for the Galactic pole at  $R \sim 22$ . A corrected isoplanatic angle twice as large (60 arcsec in diameter, Fig. 9), yields a SC of 40 per cent at the poles, 70 per cent at average latitudes and 100 per cent near the Galactic plane. Scaling the SR versus limiting magnitude of current curvature systems, we expect a SR between 0.2 and 0.4 for this reference magnitude. At a magnitude of  $R \sim 22$ , most of the wavefront reference sources will be galaxies when observing near the Galactic pole.

## 8 TECHNICAL CHALLENGES

In the previous sections, we have shown that there are no fundamental limitations imposed by the laws of atmospheric turbulence to building a visible light AO system on a 100-m optical telescope. In this section, we shall discuss the technical difficulties which have to be addressed to build such a system.

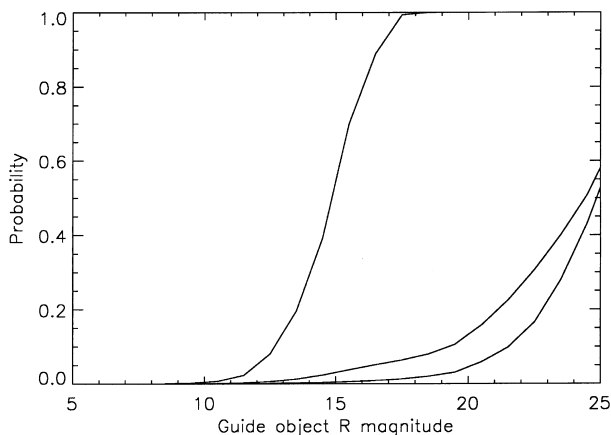


**Figure 8.** Sky coverage with four-LGS,  $\theta_3 \sim 30$  arcsec, top curve to bottom: Galactic Centre, average position and Galactic pole.

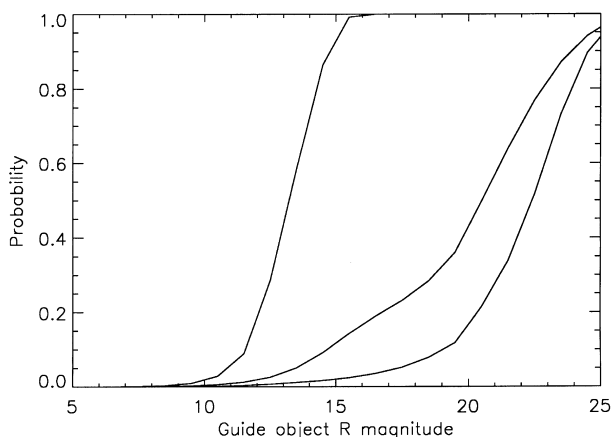


**Figure 9.** Sky coverage for the 4-LGS case,  $\theta_M \sim 60$  arcsec, top curve to bottom: Galactic disk, average position and Galactic pole.

## 8.1 Wavefront sensor

The number of subapertures of the wavefront sensor impose the use of a large detector. Centroiding computations require at least  $2 \times 2$  pixel per subaperture. For 16-cm subapertures, this means that the wavefront sensor detector must have at least  $1250 \times 1250$  pixel. Moreover, if guard pixels are used, this number could increase to  $2500 \times 2500$  ( $4 \times 4$  pixel per subaperture). The pyramid wavefront sensor concept (Ragazzoni & Farinato 1999) requires only  $2 \times 2$  per sampling area and therefore could be an interesting alternative to a Shack-Hartmann (SH) sensor. The detector noise requirement could be loosened slightly from the  $1e^-$  level we have used, if bright LGSs can be created in the atmosphere. This is, however, unlikely, since saturation problems in the sodium layer will arise (see Section 7.1).

Currently, the state-of-the-art detectors for wavefront sensors have  $128 \times 128$  pixels (Feautrier et al. 2000). The required number of pixels could, however, be reduced by two means. One could use a curvature wavefront sensing method, coupled to a CCD detector. This approach has been proposed by Beletic, Dorn & Burke (1999) and has the advantage of reducing the number of pixels needed on the detector to one per subaperture. This would bring the total required number of pixels to  $\sim 625 \times 625$ , which is realistic. It does not seem possible, with current technology, to produce a bimorph mirror (usually associated with curvature sensors) with 500 000 actuators. This problem could be solved by coupling a curvature sensor to a piezo-stack deformable mirror, but the approach clearly deserves more study.

The readout rate of the wavefront sensor detector (SH) can be obtained by scaling the typical current framerate in the IR ( $\sim 200$  Hz) to the visible. We obtain a frame rate of  $\sim 1.5$  kHz. Therefore, there is a choice to be made between a smaller number of pixels but a high frame-rate, and a larger but slower system.

Both a large number of pixels and a high readout speed can be achieved by butting small chips together, with multiple readout ports (as in the Nasmyth Adaptive Optics System wavefront sensor, Feautrier et al. 2000), or even more efficiently by adapting the CCD designing technique described in Beletic et al. (1999) to Shack-Hartmann systems, which allows a very efficient parallelization of the readout process. Therefore the wavefront sensor detector should not be technically the most challenging part of the AO system.

## 8.2 Deformable mirror

With a typical DM diameter of 0.5 m, which could be feasible on a 100-m telescope (Dierickx et al. 1999), the spacing requirement between the DM actuators would be 0.8 mm. This value is ten times smaller than on existing DMs. Therefore, the production of a DM with 500 000 actuators clearly requires new methods. Current development based on MOEMS (micro-opto-electro-mechanical systems) could lead to spacings down to 0.3 mm (e.g. Bifano et al. 1997; Vdovin, Middelhoeck & Sarro 1997; Roggeman et al. 1997), making possible a DM size of  $\sim 20$  cm. One of the key issues in the design of these DMs is the required stroke. Assuming an outer scale of turbulence of 25 m and a von Kármán model, a stroke of  $\pm 5 \mu\text{m}$  ( $3\sigma$ ) would be sufficient. However, the actual turbulence spectrum at low spatial frequencies must be measured on 8-m class telescopes for realistic estimates of the required stroke.

## 8.3 Computing power

By using Moore's law, which states that the computing power



doubles every 1.5 yr, the computing power in 20 yr will be increased by a factor of  $10^4$ .

Current wavefront computers have a delay smaller than 200  $\mu\text{s}$ , which is compatible with use in the visible (Rabaud et al. 2000). The required computing power increase can therefore be estimated as the squared ratio of the number of controlled actuators:

$$\gamma = \left( \frac{N_{\text{ELT}}}{N_{\text{IR-AO}}} \right)^2, \quad (7)$$

where  $N_{\text{IR-AO}}$  is the number of actuators of current IR AO systems (200), and  $N_{\text{ELT}}$  the number of actuators for the ELT (500 000). We get  $\gamma \sim 6 \times 10^6$ . However, this does not take into account that the cross-talk between actuators will be negligible for actuators far away from each other and therefore the interaction matrix will be very sparse. This will reduce significantly the computing load. If, for example, the interaction matrix (Boyer, Michaud & Rousset 1990) can be broken up into 6 times  $100 \times 100$  matrices, the likely evolution in technology would provide adequate power in 20 yr.

Another possibility would be to use curvature sensing, in which the interaction matrix is almost diagonal (if no modal control is employed), minimizing the computing power requirements. However, this approach, as noted earlier, seems to be prohibited by the availability of large bimorph mirrors.

## 8.4 Optics

The use of a small pitch between the actuators of the DM allows the use of a small pupil diameter: with a pitch of 300  $\mu\text{m}$ , the pupil size is 187 mm. This facilitates the imaging of the pupil on the wavefront sensor detector. Indeed, with 625 subapertures across the pupil, the WFS detector size is roughly 25 mm (assuming 2 pixel per sub-aperture and 20  $\mu\text{m}$  pixels). The reduction factor from the pupil to the detector is then 7.5, which is not a problem if each subaperture has a FOV of a few arcsec.

Atmospheric dispersion (AD) correction is currently an unsolved problem and has to be tackled at the level of telescope design. For example, AD produces an elongation of the object of 184 mas (if AD is not corrected, assuming imaging between 0.5 and 0.6  $\mu\text{m}$ , at a zenith angle of  $30^\circ$ ) which is unacceptably high. The design of the AD corrector will be challenging, since an optimal combination of glasses, allowing a correction with an accuracy better than 1 mas, must be found. The physical sizes of these AD correctors is also a problem, because of the large size of the optics. The required precision puts severe constraints on the measurement of atmospheric parameters (air temperature, humidity, pressure).

For the multiNGS scheme this problem is even more crucial, since the NGSs must be far apart to increase the sky coverage, and will therefore suffer immensely from AD. The multiLGS has the advantage of being insensitive to AD, because the sources are highly monochromatic.

If proper correctors cannot be built for technological reasons, narrow-band operation of the telescope should be used if the highest spatial resolution is required: at  $30^\circ$  from zenith a bandpass of 0.4 nm produces a dispersion of  $\sim 1$  mas, if no correction is made. The use of 3D detectors (e.g. integral field spectrographs) would solve the problem, since images in different colours can then be disentangled.

In the multiNGS case, if anisoplanatism limits the correction

and the sources do not benefit from AO correction, non-common path aberrations between the sources will be difficult to maintain.

## 8.5 Laser spot elongation

The atmospheric sodium layer is roughly 10 km thick (e.g. Papen, Gardner & Yu 1996). This causes the LGS to be extended, for subapertures which are not on the optical axis of the telescope (assuming a projection of the LGS from behind the secondary mirror of the telescope). The apparent size of a laser spot is given by simple geometry:

$$\theta_{\text{spot}} \sim \frac{\Delta H d}{H_{\text{Na}}^2}, \quad (8)$$

where  $\Delta H$  is the thickness of the sodium layer (10 km),  $H_{\text{Na}}$  the altitude of the sodium layer ( $\approx 90$  km),  $d$  is the separation of the beam projector and the considered subaperture. With  $d = 50$  m we get  $\theta_{\text{spot}} \sim 13$  arcsec. Since the multiple LGSs will be off-axis, the spots will be even more elongated. This is clearly too large for standard wavefront sensors, which typically have a field of view of 2–3 arcsec. Several methods have been proposed to eliminate spot elongation. The conceptually simplest is to use a pulsed laser and to select only a small portion of the laser stripe by filtering the photons coming from the LGS through a time gate. This has the advantage of being technically simple, at the cost of the effective brightness of the LGS. Other solutions have been proposed in the literature (e.g. Beckers 1992), improving the previous scheme by shifting the wavefront sensor measurements synchronously with the propagation of the beam in the sodium layer, thus removing the loss of photons at the price of complexity. Other less technically challenging solutions should certainly be investigated.

## 9 CONCLUSIONS

The systems are summarized in Table 5. Although a realization of an adaptive optical system working with a 100-m telescope in the visible represents a technical challenge, it is shown here that a very large aperture would open a number of new possibilities and AO correction becomes feasible for a significant fraction of the sky. The new approaches involve either the use of several widely spaced bright NGS (in the near IR) or a very faint NGS combined with few LGS. In both cases a 3D tomographic measurement of instantaneous phase screens is needed. Wavefront correction will be made with few (2–3) DMs conjugated to the optimum heights;

**Table 5.** Summary of the studied systems. The system NGS (1) is based on three NGS with a wide FOV (6 arcmin) to search for guide stars. The wavefront sensing is done in open loop. NGS (2) is also a three-NGS system, but optimized for the near IR. The LGS stands for the four-LGS system optimized for the visible.

	NGS (1)	NGS (2)	LGS
Wavelength ( $\mu\text{m}$ )	0.5	1.25	0.5
Strehl ratio (peak)	0.6	0.85	0.6
Max corrected FOV <sup>(1)</sup>	$\sim 60''$	$3'$	$60''$
Sky coverage <sup>(2)</sup>	60%	30%	70%
Number of NGS	3	3	1
Number of LGS	0	0	4
Technical difficulty	very high	low	medium

<sup>(1)</sup>Limited by residual anisoplanatism.

<sup>(2)</sup>With a Strehl ratio of 0.2, average Galactic latitude.

in this way the FOV size is increased  $\sim 8$  times compared to the single-DM AO systems, and FOV diameter may reach 1 arcmin in the visible. Additional criteria for site selection related to operation in this mode are formulated.

## ACKNOWLEDGMENTS

The authors would like to thank Roberto Ragazzoni for many useful discussions and Johan Fynbo for his data on the magnitude distribution of galaxies. This paper benefited from many discussions with B. Delabre, Ph. Dierickx and R. Gilmozzi regarding the design of 100-m telescopes. We are also grateful to an anonymous referee for improving the quality of this paper. This work was done with the help of the European TMR network ‘Laser guide star for 8-metre class telescopes’ of the European Union, contract #ERBFMRXCT960094.

## REFERENCES

- Andersen T. et al., 1999, in Andersen T., Ardeberg A., Gilmozzi R., eds, Proc. Workshop on Extremely Large Telescopes, Bäckaskog Castle, Sweden. ESO, Garching bei München, Germany, p. 72
- Arnouts S., D’Odorico S., Cristiani S., Zaggia S., Fontana A., Giallongo E., 1999, *A&A*, 341, 641
- Azouit M., Vernin J., 1980, *J. Atmos. Sci.*, 37, 1550
- Beckers J. M., 1988, in Ulrich M.-H., ed., ESO Conf on very large telescopes and their instrumentation, Vol. 2. ESO, Garching bei München, Germany, p. 693
- Beckers J. M., 1992, *Appl. Opt.*, 31, 6592
- Beletic J. W., Dorn R. J., Burke B., 1999, in Amico P., Beletic J. W., eds, Proc. ESO workshop on Optical Detectors for Astronomy. Kluwer, Dordrecht
- Bifano T. G., Mali R. K., Dorton J. K., Perreault J., Vandelli N., Horenstein M. N., Castanon D. A., 1997, *Opt. Eng.*, 36, 1354
- Boyer C., Michaud V., Rousset G., 1990, *Proc. SPIE*, 1237, 406
- Chun M., 1998, *PASP*, 110, 317
- Coulman C. E., Vernin J., Fuchs A., 1995, *Appl. Opt.*, 34, 5461
- Davies R. I., Hackenberg W., Ott T., Eckart A., Holstenberg H.-C., Rabien S., Quirrenbach A., Kasper M., 1998, *Proc. SPIE*, 3353, 116
- Dierickx P., Beletic J., Delabre B., Ferrari M., Gilmozzi R., Hubin N., Rigaut F., 1999, in Andersen T., Ardeberg A., Gilmozzi R., eds, Proc. of Workshop on Extremely Large Telescopes, Bäckaskog Castle, Sweden. ESO, Garching bei München, Germany
- Feautrier S. et al., 2000, *Proc. SPIE*, 4007, 396
- Foy R., Labeyrie A., 1985, *A&A*, 152, L29
- Foy R., Migus A., Biraben F., Grynberg G., McCullough P. R., Tallon M., 1995, *A&AS*, 111, 569
- Fried D. L., 1966, *J. Opt. Soc. Am.*, 56, 1380
- Fried D. L., 1982, *J. Opt. Soc. Am.*, 72, 52
- Fried D. L., Belsher J. F., 1994, *J. Opt. Soc. Am. A*, 11, 277
- Fuchs A., Vernin J., 1993, Final report on parscas 1992 and 1993 campaigns. Tech. Rep. VLT - TRE - UNI - 17400 - 0001. ESO, Garching bei München, Germany
- Fugate R. Q., et al., 1994, *J. Opt. Soc. Am. A*, 11, 310
- Fusco T., Conan J.-M., Michau V., Mugnier L. M., Rousset G., 1999, *Proc. SPIE*, 3763, 125
- Fynbo J. U., Freudling W., Moller P., 2000, *A&A*, 355, 37
- Gilmozzi R. et al., 1998, *Proc. SPIE*, 3352, 778
- Graves J. E., Northcott M. J., Roddier F. J., Roddier C. A., Close L. M., 1998, *Proc. SPIE*, 3353, 34
- Jacobsen B., Martinez T., Angel R., Lloyd-Hart M., Benda S., Middleton D., Friedman H., Erbert G., 1994, *Proc. SPIE*, 2201, 342
- Johnston D. C., Welsh B. M., 1994, *J. Opt. Soc. Am. A*, 11, 394
- Le Louarn M., Foy R., Hubin N., Tallon M., 1998, *MNRAS*, 295, 756
- Martin F., Tokovinin A., Ziad A., Conan R., Borgnino J., Avila R., Agabi A., Sarazin M., 1998, *A&A*, 336, L49
- Max C. E. et al., 1997, *Sci*, 277, 1649
- Milonni P. W., Fugate R. Q., Telle J. M., 1998, *J. Opt. Soc. Am. A*, 15, 217
- Mountain M., 1997, *Proc. SPIE*, 2871, 597
- Papen G. C., Gardner C. S., Yu J., 1996, in Wizinowich P., ed., OSA conf. on Adaptive Optics, 13, 96
- Pilkington J. D. H., 1987, *Nat*, 330, 116
- Rabaud D. et al., 2000, *Proc. SPIE*, 4007, 659
- Ragazzoni R., 1996, *A&A*, 305, L13
- Ragazzoni R., 1999, *A&AS*, 136, 205
- Ragazzoni R., Farinato J., 1999, *A&A*, 350, L23
- Ragazzoni R., Marchetti E., Rigaut F., 1999, *A&A*, 342, L53
- Rigaut F., Gendron E., 1992, *A&A*, 261, 677
- Rigaut F., et al., 1998, *PASP*, 110, 152
- Robin A., Crézé M., 1986, *A&A*, 157, 71
- Roddier F., 1981, in Wolf E., ed., *Progress in optics*, Vol. 19, North-Holland Publishing Co., Amsterdam, p. 281
- Roddier F., 1999, *Adaptive optics in astronomy*, Cambridge Univ. press, Cambridge
- Roddier F., Roddier C., Roddier N., 1988, *Proc. SPIE*, 976, 203
- Roggeman M. C., Bright V. M., Welsh B. M., Hick S. R., Roberts P. C., Cowan W. D., Comtois J. H., 1997, *Opt. Eng.*, 36, 1326
- Rousset G., 1994, in Alloin D. M., Mariotti J.-M., eds, *Adaptive optics for astronomy*. Kluwer, Dordrecht, p. 115
- Sandler D., 1999, in Roddier F., ed., *Adaptive optics in astronomy*. Cambridge Univ. press, Cambridge, p. 331
- Sarazin M., 1996, in Cullum M., ed., *Optical Society of America (OSA)/ESO topical meeting on adaptive optics*. ESO, Garching bei München, Germany, p. 439
- Sasiela R. J., 1994, in Brekhovskikh L., Felsen L., Haus H. A., eds, *Electromagnetic wave propagation in turbulence*. Springer-Verlag
- Stockman H. S., 1997, *The Next Generation Space Telescope - Visiting a time when galaxies were young*. The Association of Universities for Research in Astronomy, Inc., Washington, DC
- Tallon M., Foy R., 1990, *A&A*, 235, 549(TF90)
- Tallon M., Foy R., Vernin J., 1992, in Ulrich M.-H., ed., *Progress in telescope and instrumentation technologies*. ESO, Garching bei München, Germany, p. 517
- Tokovinin A., Le Louarn M., Sarazin M., 2000, *J. Opt. Soc. Am. A*, in press
- Tyler G. A., 1994, *J. Opt. Soc. Am. A*, 11, 325
- Vdovin G., Middelhoek S., Sarro P. M., 1997, *Opt. Eng.*, 36, 1382
- Williams R. E. et al., 1996, *AJ*, 112, 1335

This paper has been typeset from a  $\text{\TeX}/\text{\LaTeX}$  file prepared by the author.